Electronic Supplementary Information

for

Mechanised Lubricating Silica Nanoparticles for On-Command

Cargo Release on Simulated Surface of Joint Cavity

Xiaolong Tan[†], Yulong Sun[†], Tao Sun and Hongyu Zhang[*]

State Key Laboratory of Tribology, Department of Mechanical Engineering, Tsinghua

University, Beijing 100084, China.

[†] These authors contributed equally to this work.

[*]Correspondence to Dr Hongyu Zhang

State Key Laboratory of Tribology, Department of Mechanical Engineering,

Tsinghua University, Beijing 100084, China.

Tel: +86 010 62796053

Fax: +86 010 62781379

E-mail: zhanghyu@tsinghua.edu.cn

Contents

1. Materials and Methods

Calix[4]arenes (C[4]A, 98%), cetyltrimethylammonium bromide (CTAB, 98%), betaine hydrochloride (98%) and 3-aminopropyltriethoxysilane (APTES, 98%) were purchased from J&K Scientific Co., China. NaOH (99%), tetraethyl orthosilicate (TEOS, 98%), chloroform (99%), hydrochloric acid (HCl, 37%), conc. H_2SO_4 (98%), N,N-dimethylformamide (DMF, 99%), toluene (99.5%) and methanol (99%) were purchased from Beijing Chemical Reagent Co., China. Thionyl chloride (99%) was purchased from Aladdin Co., China. Rhodamine B (RhB, 96%) and PBS solution (pH 7.2–7.4) were purchased from Solarbio Co., China. All the reagents were used as received. Unless otherwise noted, all reactions were performed under nitrogen atmosphere and in dry solvents.

Transmission electron microscopy (TEM) was carried out on an H-7650B instrument (HITACHI) to examine the morphology of the nanoparticles. Dynamic light scattering (DLS) was measured by using a Zetasizer Nano ZS size analyser (Malvern Instruments, Malvern, UK) equipped with a 633 nm He-Ne laser to test the hydrated radius and zeta potential of samples. Fourier transform infrared (FT-IR) spectrum was recorded by using a Nexus 670 Spectrometer (Thermo-Nicolet, Madison, WI, USA). The range of wavelength was from 4000 cm^{-1} to 400 cm^{-1}. Nuclear magnetic resonance spectrum (NMR) was recorded by using an Ascend 400 MHz (Bruker Co. Ltd., Billerica, USA). X-ray photoelectron (XPS) spectrum was obtained by using an Escalab 250 Xi spectrometer (Thermo Scientific, Waltham, MA, USA) and the binding energy was calibrated against the O1s peak at 523 eV. X-ray diffraction spectrum (XRD) was scanned by using a Bruker AXS D8 Diffractometer (Bruker, Karlsruhe, Baden-Württemberg, Germany) with an incident angle (2θ) from 0.6° to 10°. Thermogravimetric analysis (TGA) was conducted on a Q5000 instrument (TA Instruments, New Castle, DE, USA) at a heating rate of 10 °C /min from 25 °C to 800 °C. N_2 adsorption−desorption isotherm (BET) and pore size distribution (BJH) were carried out by using Quantachrome SI-MP equipment (Quantachrome, Boyton beath, CA,

USA). The tribological tests were conducted using a Bruker UMT-5 universal micro-tribology (Bruker, Billerica, MA, USA). The amount of RhB released was evaluated by a UV-vis spectrophotometer (UV-8000s, Metash Instruments, Shanghai, China). The absorbance of *in vitro* cytotoxicity tests were recorded using a microplate reader (Varioskan Flash, Thermo, Waltham, MA, USA) at 450 nm.

2. Preparation and Synthesis

2.1. Synthesis of *p*-sulfonato-calix[4]arenes (SC[4]A)[S1]

0.5 g of C[4]A was suspended in 5 mL H_2SO_4 (98%) at room temperature and stirred for 1 h. The reaction was an intensely exothermic reaction. After being cooled to room temperature, 10 mL saturated NaCl solution was added dropwise into the solution. The solution was boiled and refluxed for 5 minutes then cooled to room temperature. A water-soluble precipitate was obtained by filtration and the crude solid was purified by recrystallization (the yield: 62%).
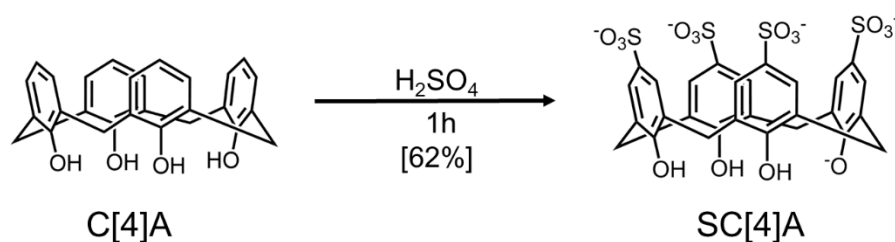
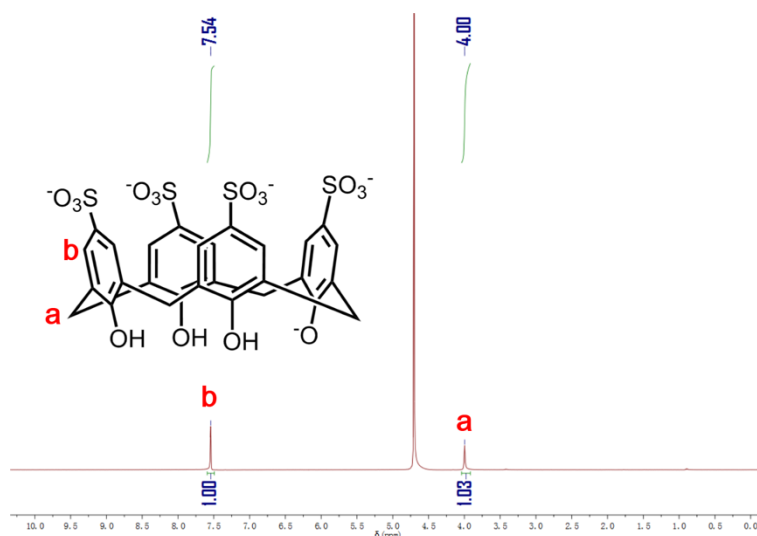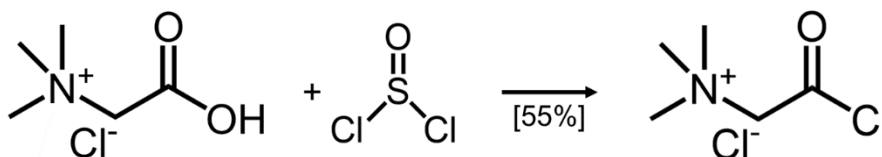**Scheme S1.** Synthesis route to **SC[4]A.**

Figure S1. ^1H NMR Spectrum of **SC[4]A.**

2.2. Synthesis of N-chlorobetainyl chloride

1.2 mL thionyl chloride was added into 0.9 g of well-dried betaine hydrochloride at room temperature. The reaction was an intensely exothermic reaction and finished when gas evolution ceased. The excessive thionyl chloride was removed by rotary evaporator. The resulting product was dried under vacuum overnight to obtain N-chlorobetainyl chloride (the yield: 55%). Betaine hydrochloride: ^{13}C NMR (125 MHz, 25 °C, D_2O) δ 53.38, 66.36, 169.18. FT-IR (ATR): 1631, 1496, 1412, 1240, 986, 891, 713 cm^{-1}. N-chlorobetainyl chloride: ^{13}C NMR (125 MHz, 25 °C, D_2O) δ 53.83, 63.85, 167.18, 44.80, 190.96. FT-IR (ATR): 1730, 1479, 1404, 1207, 987, 883, 677 cm^{-1}. These spectra were shown in **Figure S2–S4.**

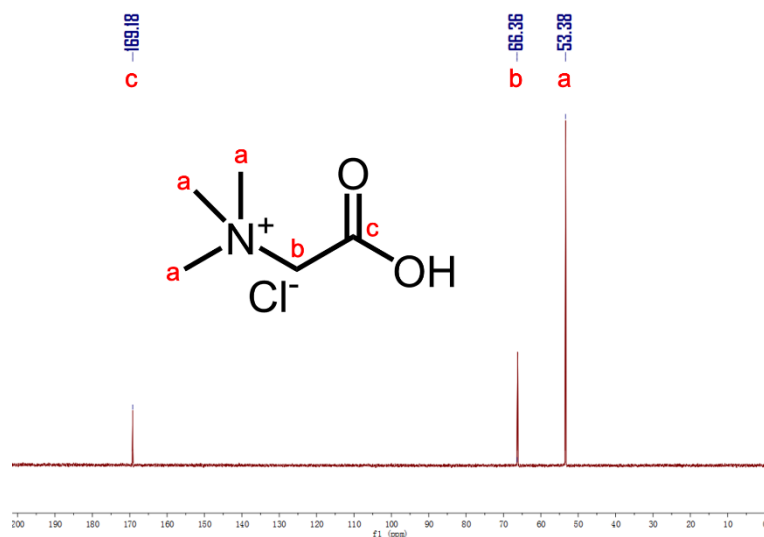**Scheme S2.** Synthesis route to N-chlorobetainyl chloride.

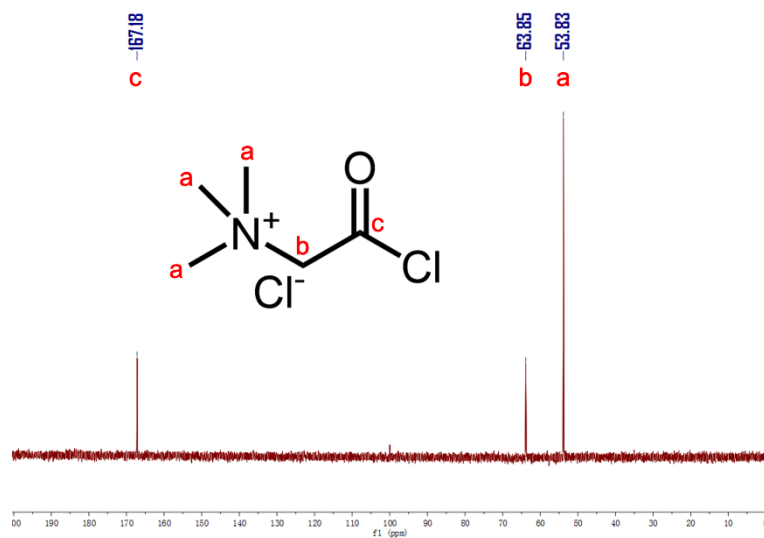**Figure S2.** ^{13}C NMR spectrum of betaine hydrochloride in D_2O at 25 ^{o}C.

Figure S3. ^{13}C NMR spectrum of N-chlorobetainyl chloride in D_2O at 25 ^{o}C.
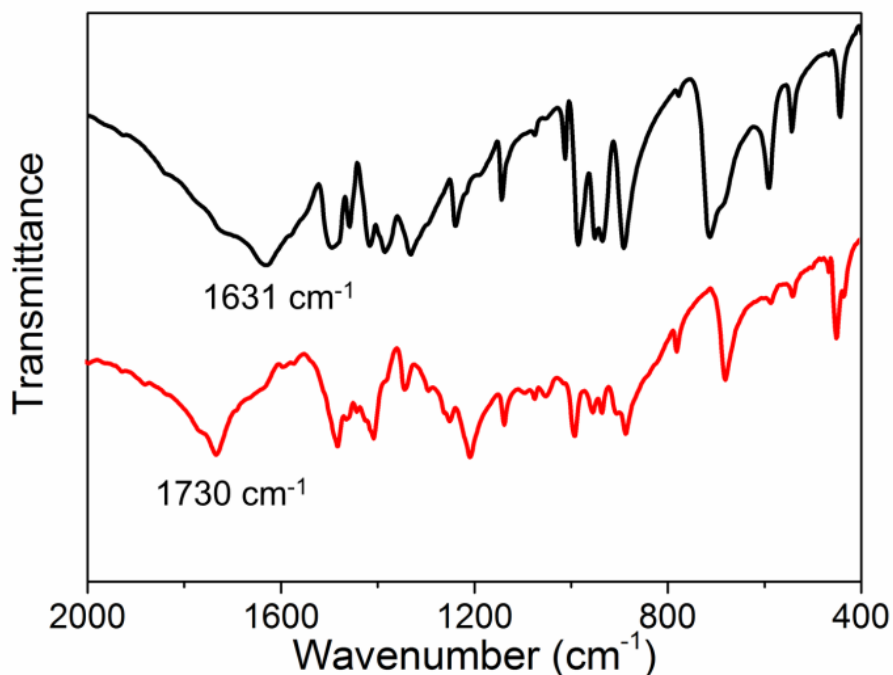
6

Figure S4. FT-IR spectra of betaine hydrochloride (black) and N-chlorobetainyl chloride (red).

2.3. Preparation of aminated mesoporous silica nanoparticles (MSNs-NH$_2$)[S2]

1.0 g of CTAB and 3.5 mL of NaOH solution (2 mol/L) were added into 480 mL deionized water and the solution was stirred at 80 °C for 30 minutes. Then, 5 mL of TEOS was added dropwise and the solution was stirred at 80 °C for another 2 h. The resulting product was collected by centrifugation (8000 rpm, 10 min), purified by washing with sufficient deionized water and methanol, and dried under vacuum to obtain MSNs with template.

1.0 g of as-made MSNs with template were dispersed by sonication in 100 mL anhydrous toluene and 5 mL APTES was injected. The solution was refluxed under 110 °C for 24 h. The resulting product was collected by centrifugation (8000 rpm, 10 min), washed with sufficient deionized water and methanol then dried under vacuum to obtain MSNs-NH$_2$ with template.

To remove the CTAB template, 1.0 g of MSNs-NH$_2$ with template were dispersed by

sonication in 100 mL methanol and 1 mL HCl (12 mol/L). The solution was stirred with refluxing at 60 °C for 24 h. Finally, the resulting product was centrifuged (8000 rpm, 10 min), washed with sufficient methanol and dried under vacuum overnight to obtain MSNs-NH$_2$.

2.4. Preparation of betaine-modified mesoporous silica nanoparticles (bMSNs)

100 mg of MSNs-NH$_2$ were dispersed by sonication in 20 mL DMF and 50 mg of N-chlorobetainyl chloride was added. The solution was stirred at 100 °C for 12 h. The resulting product was centrifuged at 8000 rpm for 10 min then washed with DMF and methanol and dried under vacuum overnight to obtain bMSNs.

2.5. Preparation of SC[4]A-capped betaine-modified mesoporous silica nanoparticles (bMSNs⊃SC[4]A)

100 mg of bMSNs were dispersed by sonication in 10 mL deionized water, then 30 mg of SC[4]A was added. The solution was stirred at room temperature for 12 h. The resulting product was centrifuged at 8000 rpm for 10 min, washed with DMF and methanol and dried under vacuum overnight to obtain bMSNs⊃SC[4]A.

3. Material Characterization

3.1. DLS

DLS was used to monitor size distribution and zeta potential of the nanoparticles (**Figure S5–S8**). The average diameters of bMSNs and bMSNs⊃SC[4]A examined by DLS were about 240 nm, larger than that of TEM (about 100 nm), because of the influence of hydrated layers on the surface of MSNs. Meanwhile, bMSNs⊃SC[4]A aggregated because SC[4]A capped on the surface of bMSNs may also have host-guest interaction with betaine molecules of other bMSNs. bMSNs showed a peak of zeta potential at 11.2 mv. But after assembly with SC[4]A, the value of the zeta potential of bMSNs⊃SC[4]A turned to –7.3 mv, due to the sulfonic acid group of SC[4]A on the surface of bMSNs⊃SC[4]A.

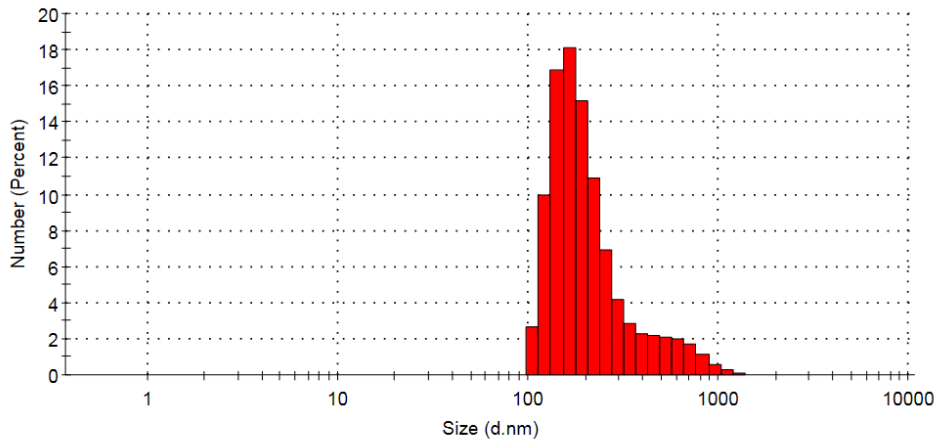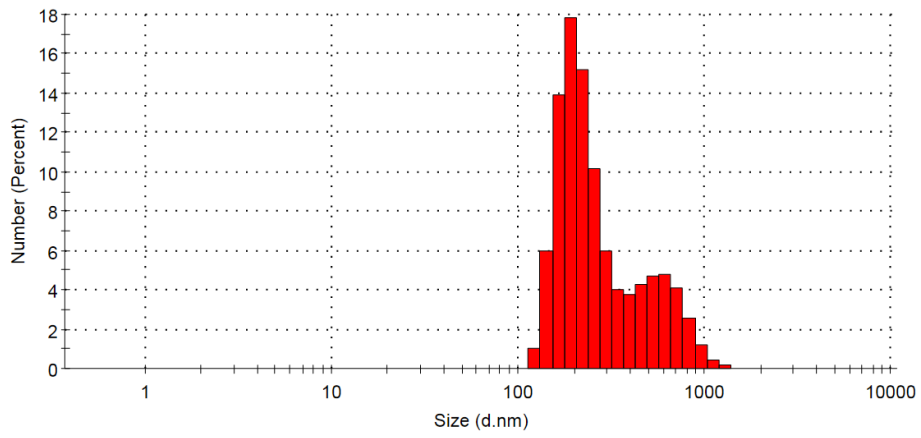**Figure S5.** Diameter distribution of bMSNs.
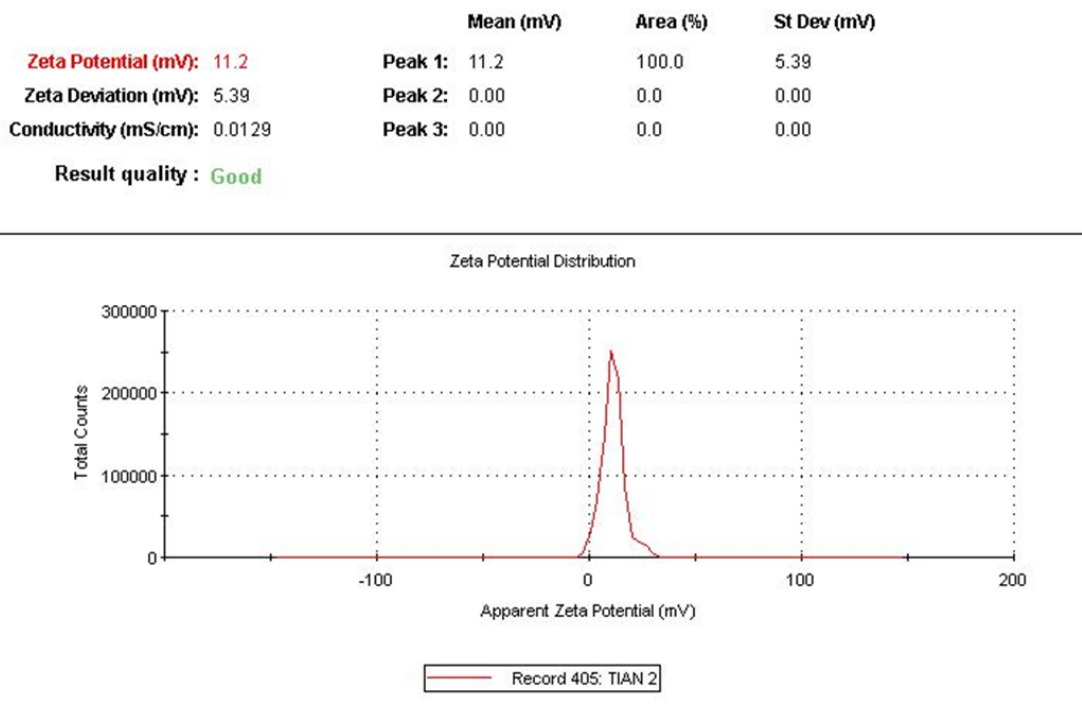

Figure S6. Diameter distribution of bMSNs⊃SC[4]A.

	Mean (mV)	Area (%)	St Dev (mV)
Zeta Potential (mV): 11.2	Peak 1: 11.2	100.0	5.39
Zeta Deviation (mV): 5.39	Peak 2: 0.00	0.0	0.00
Conductivity (mS/cm): 0.0129	Peak 3: 0.00	0.0	0.00
Result quality : Good			

Figure S7. Zeta position of bMSNs.

	Mean (mV)	Area (%)	St Dev (mV)
Zeta Potential (mV): -7.30	Peak 1: -7.30	100.0	3.18
Zeta Deviation (mV): 3.18	Peak 2: 0.00	0.0	0.00
Conductivity (mS/cm): 0.0322	Peak 3: 0.00	0.0	0.00
Result quality : Good			

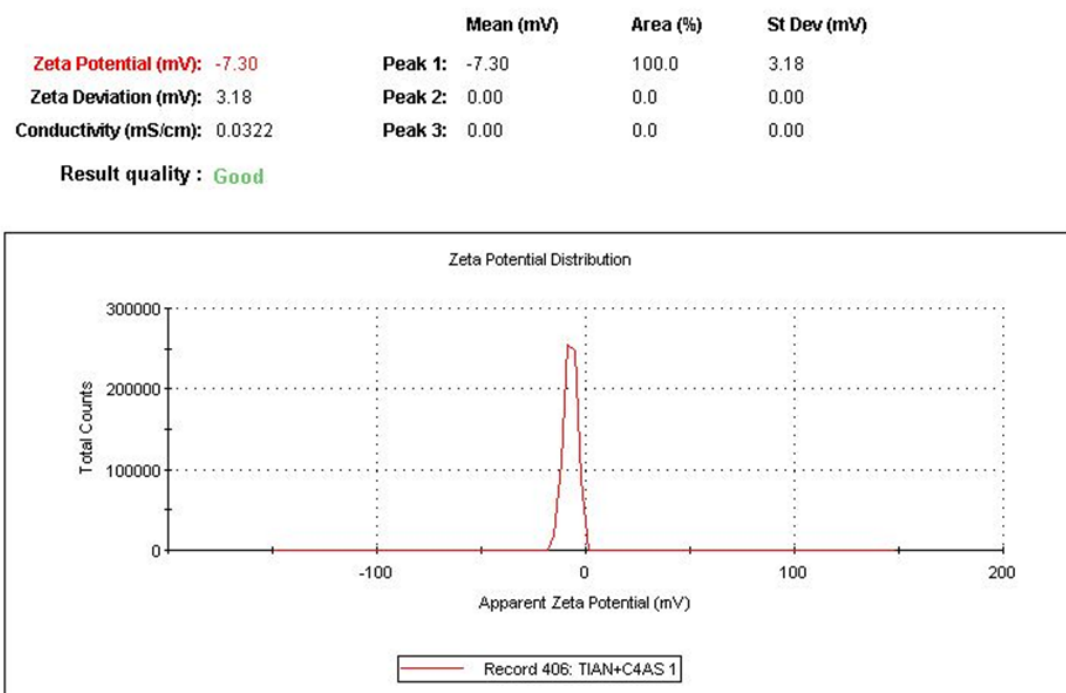**Figure S8.** Zeta position of bMSNs⊃SC[4]A.

3.2. FT-IR

FT-IR spectra were used to characterise the modification and assembly on the surface of MSNs. In **Figure S9**, a peak observed at 1635 cm^{-1} in MSNs-NH$_2$ was corresponding to the bending vibration of N–H. After modification with betaine, the stretching vibration of C=O was formed at 1634 cm^{-1}. The self-assembly does not produce any new chemical bonds, only appeared the skeleton vibration from benzene-based molecules at 1458 cm^{-1}.
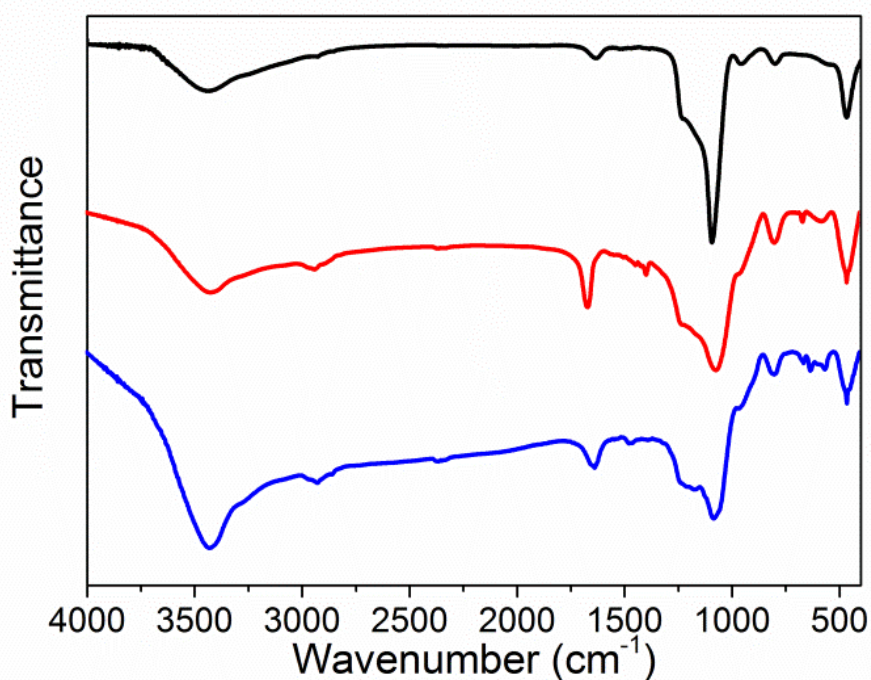

Figure S9. FT-IR spectra (from top to bottom) of MSNs-NH$_2$ (black), bMSNs (red) and bMSNs⊃SC[4]A (blue).

3.3. XPS

In the O1s region of bMSNs, two O1s peaks were observed in **Figure S10**, corresponding to Si–O (532.3 eV), C–O–C and C=O (532.6 eV). **Figure S11** showed four O1S peaks of bMSNs⊃SC[4]A. Two new kind oxygens, benzene C–O–H (533.1 eV) and SO$_3^-$ (531.9 eV), were introduced by SC[4]A.
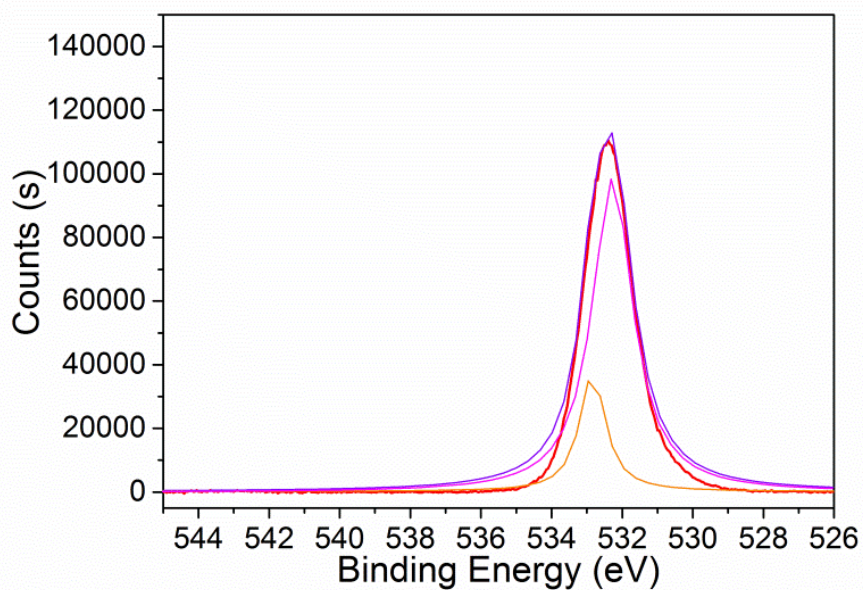
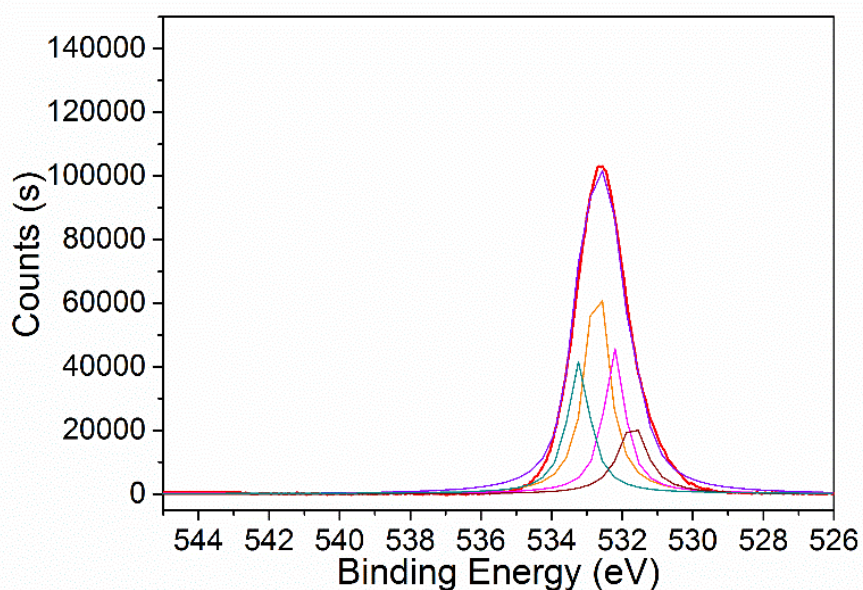**Figure S10.** XPS spectrum (O1s) of bMSNs.

Figure S11. XPS spectrum (O1s) of bMSNs⊃SC[4]A.

In the C1s region of bMSNs, three peaks were observed in **Figure S12,** corresponding to C–C and C–Si (284.6 eV), C–O and C=O (286.3 eV), and C–N (285.7 eV). In the C1s region of bMSNs⊃SC[4]A (**Figure S13**), a new peak appeared at 286.6 eV, corresponding to the C–O on benzene.
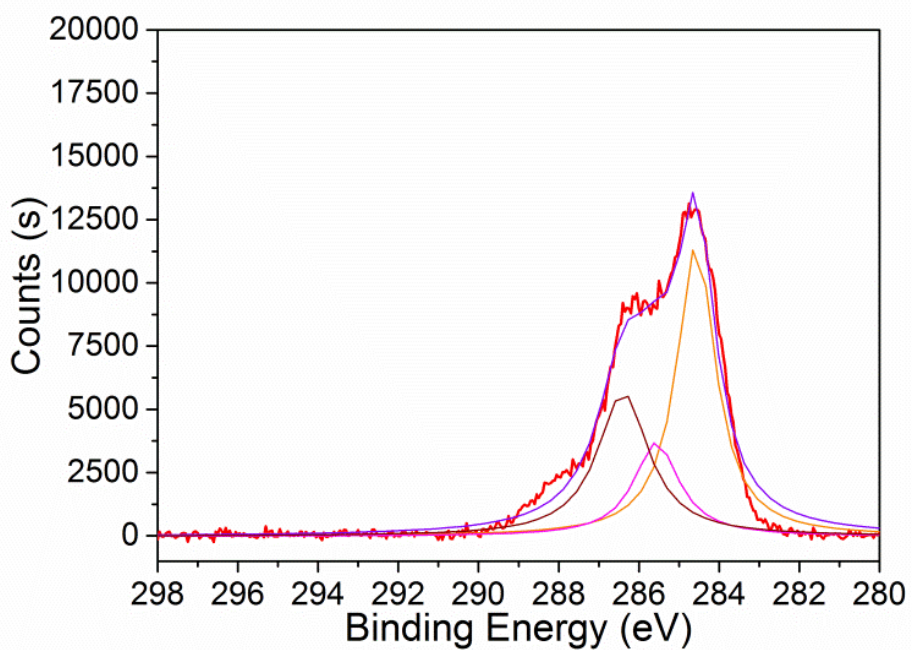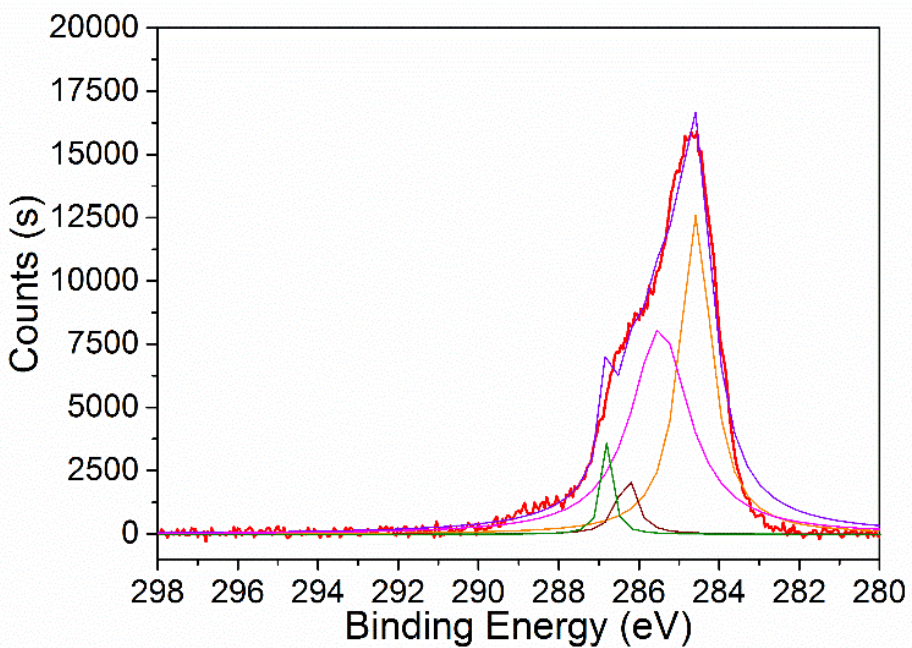
12

Figure S12. XPS spectrum (C1s) of bMSNs.

Figure S13. XPS spectrum (C1s) of bMSNs⊃SC[4]A.

After assembly with SC[4]A, sulfur was found as a new element from bMSNs⊃SC[4]A on the surface in **Figure S14**. The peak at 168 eV corresponded to S2p3/2 of SO_3^-.
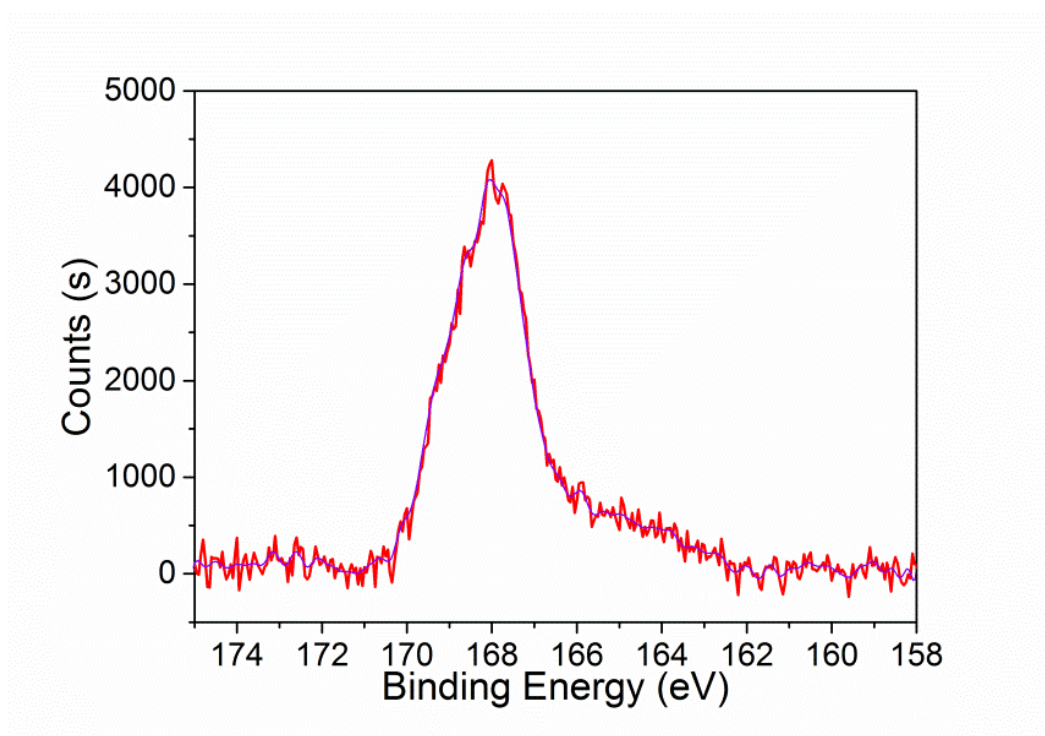
Figure S14. XPS spectrum (S1s) of bMSNs⊃SC[4]A.

3.4. TGA

TGA was used to quantitatively analyse the composition of MSN-NH$_2$, bMSN, and bMSN⊃SC[4]A. The weight loss of MSNs-NH$_2$, bMSNs, and bMSNs⊃SC[4]A was 12.88%, 21.98%, and 33.72%, respectively. The calculated composition was shown in **Table S1**.

Table S1. The composition of MSN-NH$_2$, bMSN and bMSN⊃SC[4]A.

Samples	MSN-NH$_2$	Betaine	SC[4]A
MSN-NH$_2$	100%		
bMSN	89.56%	10.44%	
bMSN⊃SC[4]A	76.08%	8.87%	15.05%

The grafting densities of betaine (ρ_b) and SC[4]A (ρ_s) on the surface of MSN were calculated as follow:

The number of nanoparticles in 1 g of MSNs (n) was calculated according to sphere volume formula (**Equation S1**):

14

$$n = \frac{1}{\rho \frac{1}{6}\pi D^3} \quad (\rho = 0.8 \ g/cm^3; D = 100nm) \ \text{(S1)}$$

The number of betaine in 1 g of MSNs (n_b) (**Equation S2**):

$$n_b = \frac{87.12\% - 78.02\%}{78.02\%} \frac{N_A}{M_b} \quad (M_b = 101 \ g/mol; N_A = 6.02 * 10^{23}/mol) \ \text{(S2)}$$

ρ_b was calculated in **Equation S3**:

$$\rho_b = \frac{n_b}{n*\pi D^2} \quad \text{(S3)}$$

By similar equation, ρ_s could also be calculated.

We got: ρ_b = 0.525 molecule/nm^2 and ρ_s = 0.122 molecule/nm^2.

ρ_s/ρ_b = 23%, indicating that 23% of betaine assembled with SC[4]A due to host-guest interaction.

3.5. Small-angle XRD

Small-angle XRD was used to investigate the change of microcrystalline of the nanoparticles (**Figure S15**).
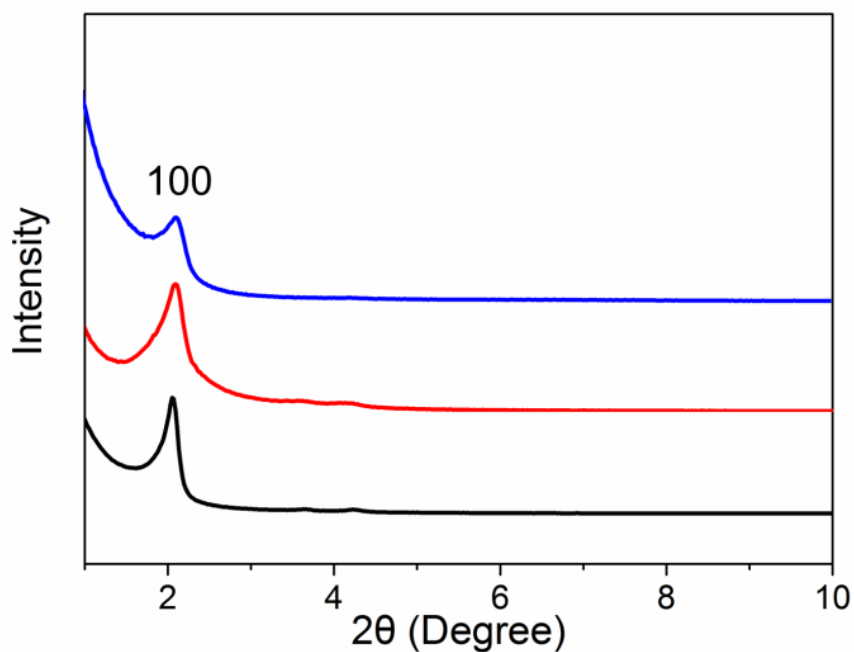

Figure S15. XRD of MSN-NH$_2$ (black), bMSN (red) and bMSN⊃SC[4]A (blue).

The distance between adjacent pores and pore diameters of MSN-NH$_2$, bMSN, and bMSN⊃SC[4]A could be calculated according to positions of the peak of (100). According to the Bragg Equation (**Equation S4**):

$$2\text{dsin}\theta = n\lambda \ (n = 1; \lambda = 1.54184 \text{ Å}) \ \ (\text{S4})$$

Interplanar spacing (**Equation S5**):

$$d = n\lambda/(2\text{sin}\theta) \ \ (\text{S5})$$

100 interplanar spacing (**Equation S6**):

$$d_{100} = \lambda/(2\text{sin}\theta) \ \ (\text{S6})$$

Pore distance (**Equation S7**):

$$a = \left(\frac{2}{1.732}\right) d_{100} = 1.155\lambda/(2\text{sin}\theta) \ \ (\text{S7})$$

The positions of the peak of (100) of MSN-NH$_2$, bMSN, and bMSN⊃SC[4]A were observed at 2.03°, 2.08°, and 2.12°, respectively. The interplanar spacing and pore distance calculated accordingly by Bragg's Law were shown in **Table S2**.

Table S2. Properties of MSN-NH$_2$, bMSN and bMSN⊃SC[4]A calculated from XRD.

Samples	Interplanar Spacing [nm]	Pore Distance [nm]
MSN-NH$_2$	4.35	5.03
bMSN	4.25	4.91
bMSN⊃SC[4]A	4.17	4.81

3.6. N$_2$ adsorption and desorption isotherm

The BET and BJH curves of MSNs-NH$_2$, bMSNs and bMSNs$\supset$SC[4]A were shown in **Figure S16–S21**.
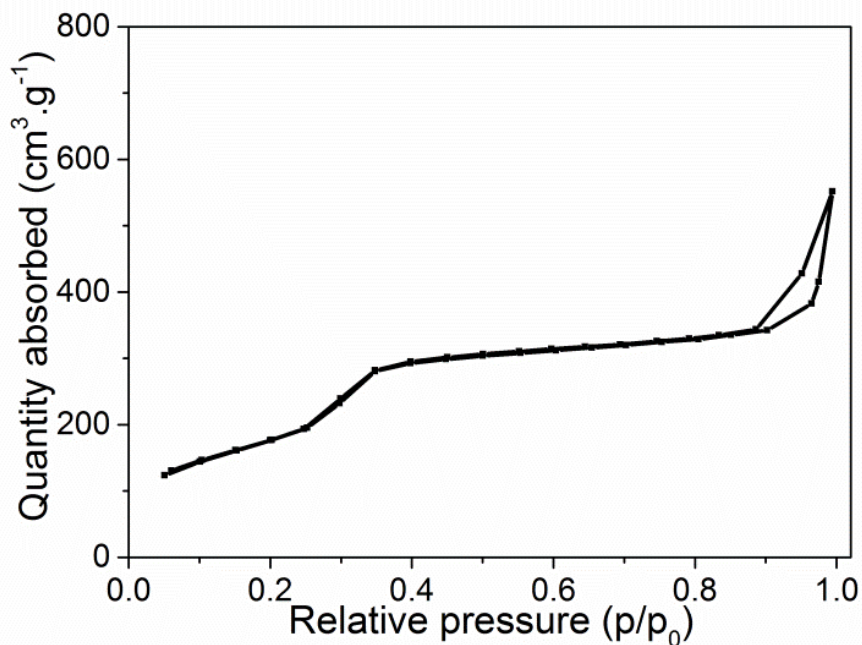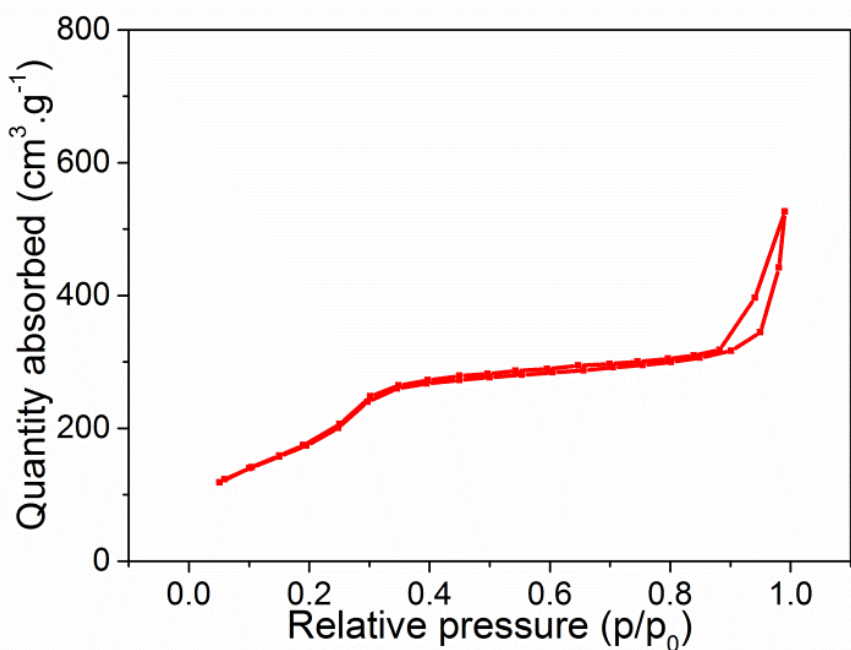

Figure S16. BET curve of MSNs-NH$_2$.

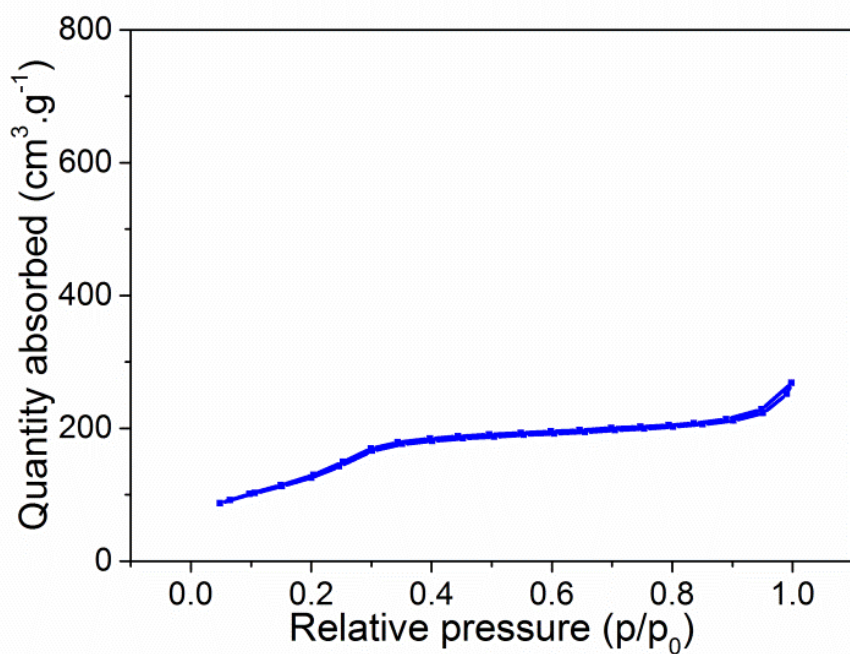**Figure S17.** BET curve of bMSNs.

Figure S18. BET curve of bMSNs⊃SC[4]A.
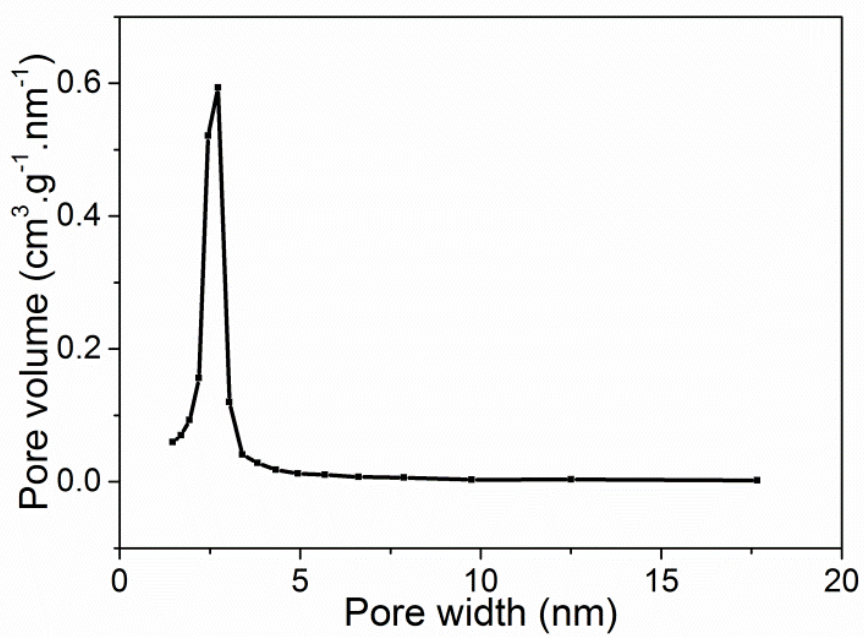

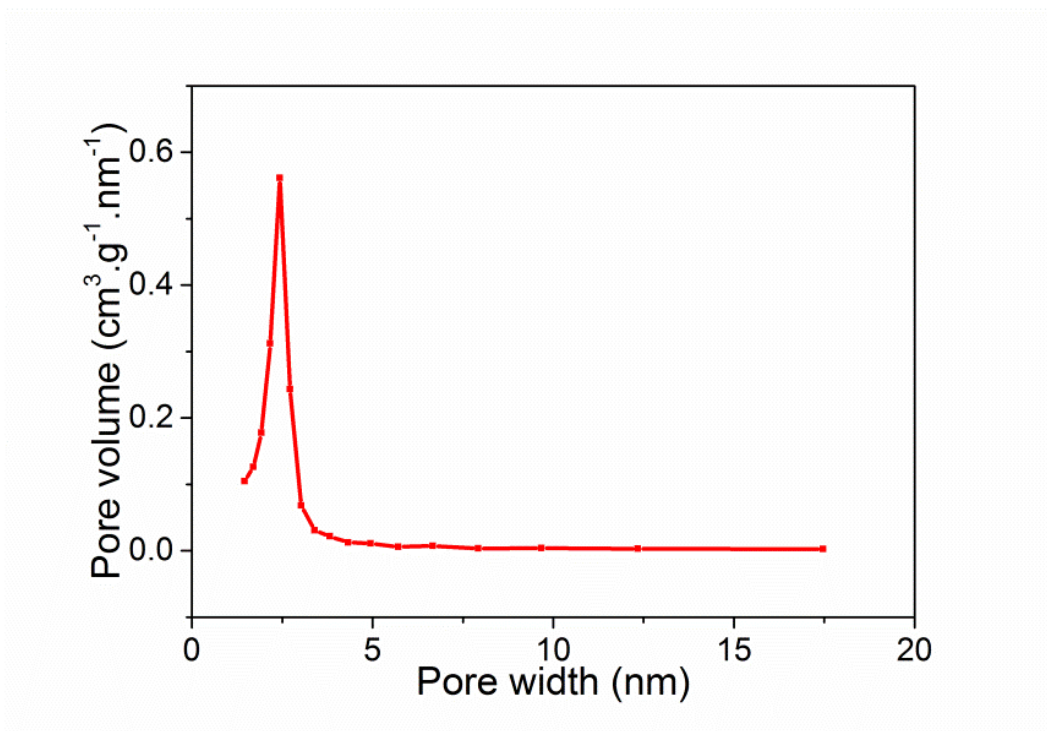**Figure S19.** BJH curve of MSNs-NH$_2$.
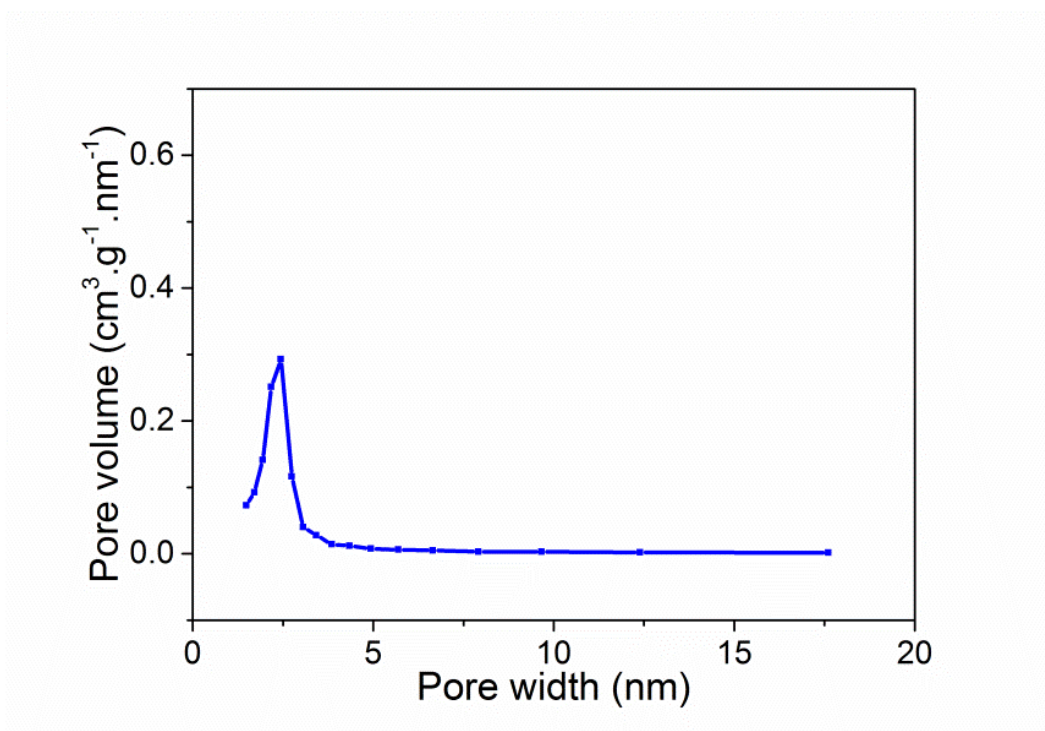
18

Figure S20. BJH curve of bMSNs.

Figure S21. BJH curve of bMSNs⊃SC[4]A.

Three methods were used to obtain the particle diameters:

D^a was obtained directly by BJH method.

D^b was calculated by averaged pore diameter (APD) method: cylindrical pores were

considered as an infinite hexagonal array (**Equation S8**):

$$APD = 1.213d_{100}((\rho V_p/(1+\rho V_p))^{1/2}) \ (\rho = 0.8 \ g/cm^3) \ (S8)$$

D^c was calculated by simple cylindrical pores model using the BET surface area (**Equation S9**):

$$D_p = 4V_p/S_{BET} \ (S9)$$

The results were shown in **Table S3**.

Table S3. Diameters of MSN-NH$_2$, bMSN and bMSN⊃SC[4]A.

Samples	S_{BET} [m^2/g]	V_p [mL/g]	$D_1{}^a$ [nm]	$D_2{}^b$ [nm]	$D_3{}^c$ [nm]
MSN-NH$_2$	831	0.969	2.72	3.49	4.66
bMSN	809	0.886	2.44	3.32	4.38
bMSN⊃SC[4]A	531	0.426	2.44	2.55	3.21

4. Tribological Tests

The lubrication property of bMSNs⊃SC[4]A was evaluated through a series of tribological tests in a reciprocating mode (oscillation amplitude: 4 mm). We investigated the lubrication property of bMSNs⊃SC[4]A under different conditions (concentration of nanoparticles, normal load, and sliding frequency). The experimental conditions were attempted as follows: concentration of nanoparticles (0.5 mg/mL, 1 mg/mL and 5 mg/mL); normal load (1 N, 2 N and 3 N); sliding frequency (1 Hz, 5 Hz and 10 Hz) and test duration (15 min). The lower specimen was a polished Ti6Al4V disk, which slid against a poly tetra fluoroethylene (PTFE) sphere pin (diameter: 8 mm), as the upper specimen. The schematic diagram was shown in **Figure S22.**
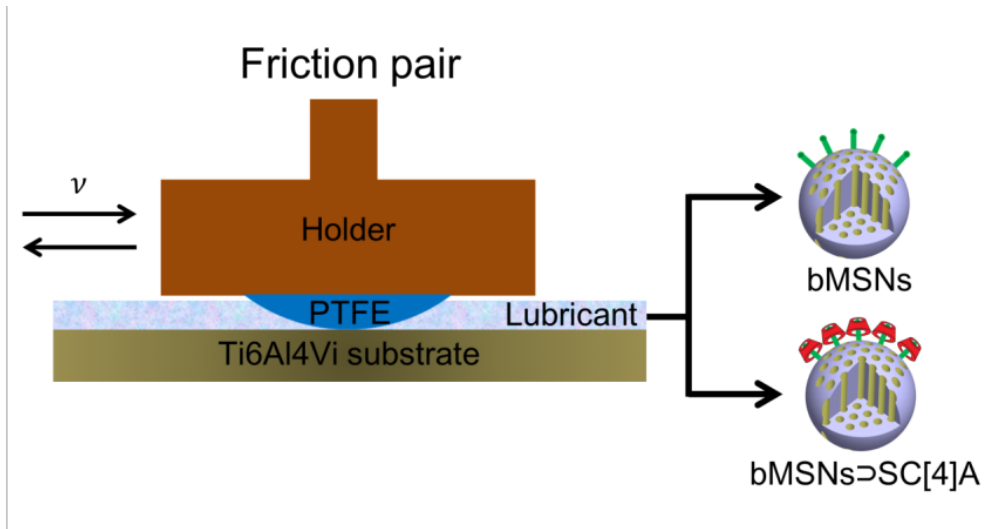
Figure S22. Schematic diagram of tribological tests.

Contact radius (c) and maximum contact pressure (σ_{Hmax}) were calculated based on Hertz theory for ball-on-flat configuration (**Equation S10 and S11**). The results were shown in **Table S4**. The maximum contact pressure in the experiments was much higher than the human joints pressure during walking (10–20 Mpa).[S3]

$$c = \sqrt[3]{\frac{3}{4}F\frac{\frac{1-\mu_1^2}{E_1}+\frac{1-\mu_2^2}{E_2}}{\frac{1}{\rho_1}+\frac{1}{\rho_2}}} \quad (S10)$$

$$\sigma_{Hmax} = \frac{1}{\pi}\sqrt[3]{6F\left(\frac{\frac{1}{\rho_1}+\frac{1}{\rho_2}}{\frac{1-\mu_1^2}{E_1}+\frac{1-\mu_2^2}{E_2}}\right)^2} \quad (S11)$$

$(\rho_1 = 4\ mm,\ \rho_2 = \infty,\ \mu_1 = 0.3,\ E_1 = 0.5\ GPa,\ \mu_2 = 0.3,\ E_2 = 114\ GPa)$

Table S4. Contact radius (c) and maximum contact pressure (σ_{Hmax}) under different loads.

Load [N]	c [µm]	σ_{Hmax} [MPa]
1	176	15.36
2	222	19.35
3	254	22.15

A typical Stribeck curve in **Figure S23** showed friction in fluid-lubricated contacts was a non-linear function of lubricant viscosity, sliding velocity and contact pressure. Three lubrication states were identified based on the typical progression of the Stribeck curve: hydrodynamic lubrication, mixed lubrication and boundary lubrication. Generally, the COF changed only slightly with the variety of friction conditions, when lubricated under boundary lubrication state. According to our experimental results, we can predict the contact pair was lubricated under boundary lubrication state.
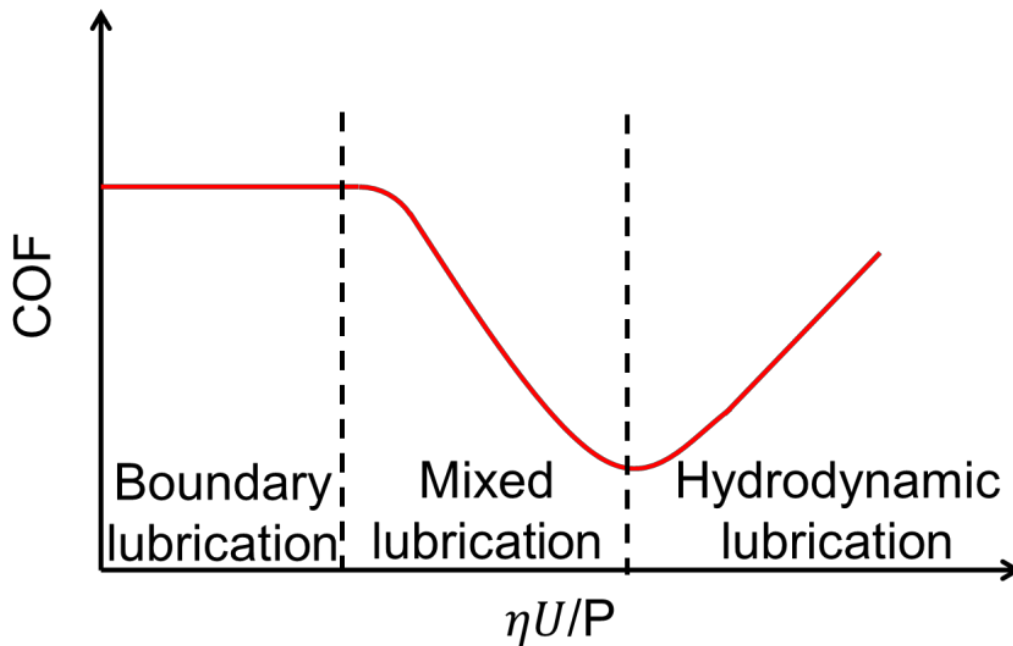

Figure S23. Typical Stribeck curve: the curve indicated the transformation of lubrication states corresponding with the working conditions, originally designed for friction between journey bearings, then extended to other types of contacts. The dimensionless bearing parameter (ηU/P) reflected the working conditions, where η was the lubricant viscosity, U was the sliding velocity, and P was the average pressure.

The surface morphology of the tribopairs is tested with bMSNs and bMSNs⊃SC[4]A by UMT. Figure S24, S25 show SC[4]A coated MSNs can effectively reduce the wear of the surfaces of tribopairs.
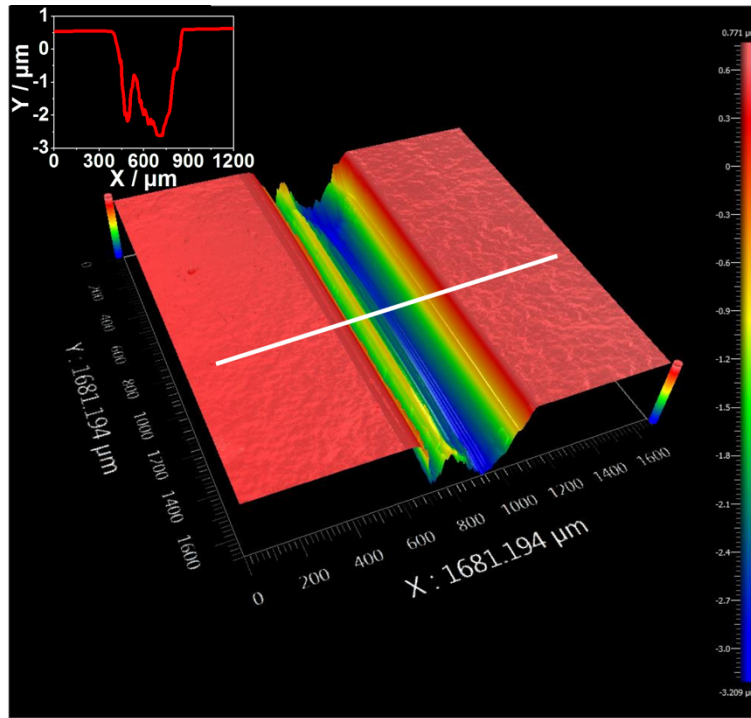
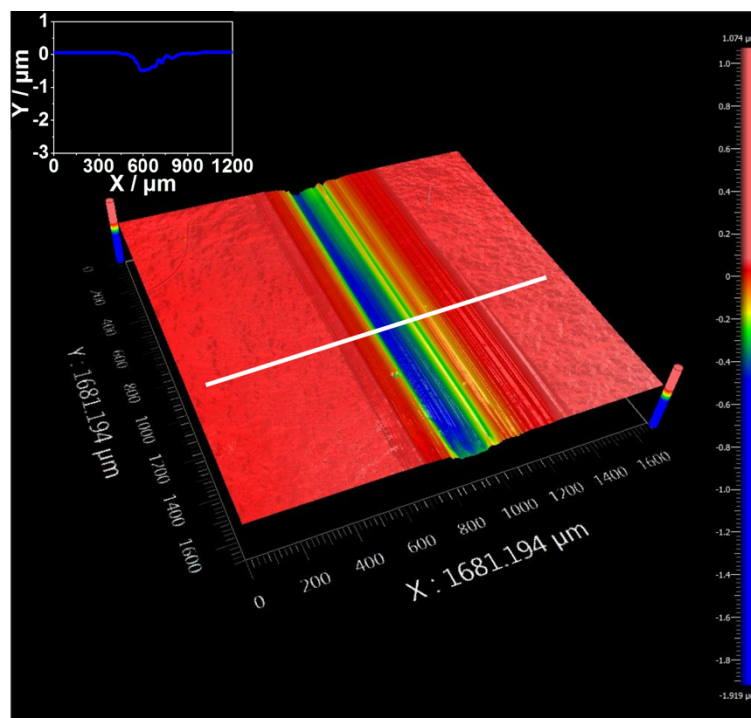**Figure S24**. The surface morphology of the tribopairs with bMSNs.

Figure S25. The surface morphology of the tribopairs with bMSNs⊃SC[4]A.

5. Cargo Loading and Controlled Release Experiments

5.1. Cargo loading and SC[4]A assembly

20 mg of bMSNs was suspended in 10 mL of RhB solution (0.5 mmol/L) in a flask and dispersed uniformly by sonication. The solution was stirred away from the light at room temperature for 24 h. For the cargo loading of bMSNs⊃SC[4]A, 20 mg of SC[4]A was added to the mixture and stirred away from the light at room temperature for another 24 h. The bMSNs@RhB and bMSNs⊃SC[4]A@RhB were separated respectively by centrifugation (8000 rpm, 10 min), washing thoroughly with deionized water, and dried under vacuum overnight. The loading capacity of bMSNs and bMSNs⊃SC[4]A was calculated to be 5.76% and 8.77%, respectively, according to the **Equation S12**.

$$\text{Loading capacity(\%)} = \frac{\text{amount of loaded RhB}}{\text{amount of RhB-loaded nanoparticles}} \times 100\% \quad (S12)$$

5.2. Controlled release experiments

In vitro release profiles of cargoes (RhB molecules) from bMSNs@RhB and bMSNs⊃SC[4]A@RhB were conducted through dialysis bag diffusion at 37 °C. 10 mg of bMSNs@RhB or bMSNs⊃SC[4]A@RhB was ultrasonically dispersed in 2 mL PBS and placed into a dialysis bag (molecular weight cutoff: 8000–10,000). The dialysis bag was immersed in 8 mL PBS (illustrated in **Figure S26**). For the cargo release where we introduced competitive binding agent, we used the same method, but the dialysis bag was immersed in a mixture of 6 mL PBS and 2 mL ethylenediamine (competitive binding). For the cargo release where we introduced dynamic friction, we used the design as **Figure S27**: the tests were conducted using a Bruker UMT-5 universal micro-tribology, bMSNs⊃SC[4]A@RhB (1 mg) were encapsulated in a dialysis bag with a PTFE ball (the PTFE ball was polished with a lower surface of 3

mm diameter plane in order to increase the contact area, so that the nanoparticles could be rubbed well) and made dynamic friction against a polystyrene (PS) container in PBS solution (5 mL). The experimental conditions attempted were as follows: normal load (1 N and 4 N) and sliding frequency (1 Hz, 2 Hz and 3 Hz).
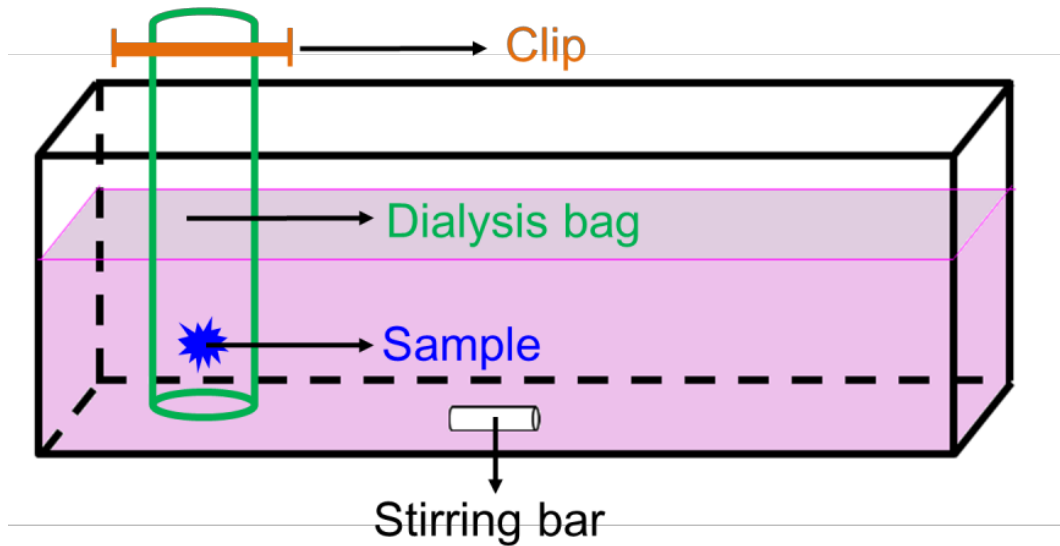

Figure S26. Illustration of no activation and competitive binding agent-activated caogo release tests.
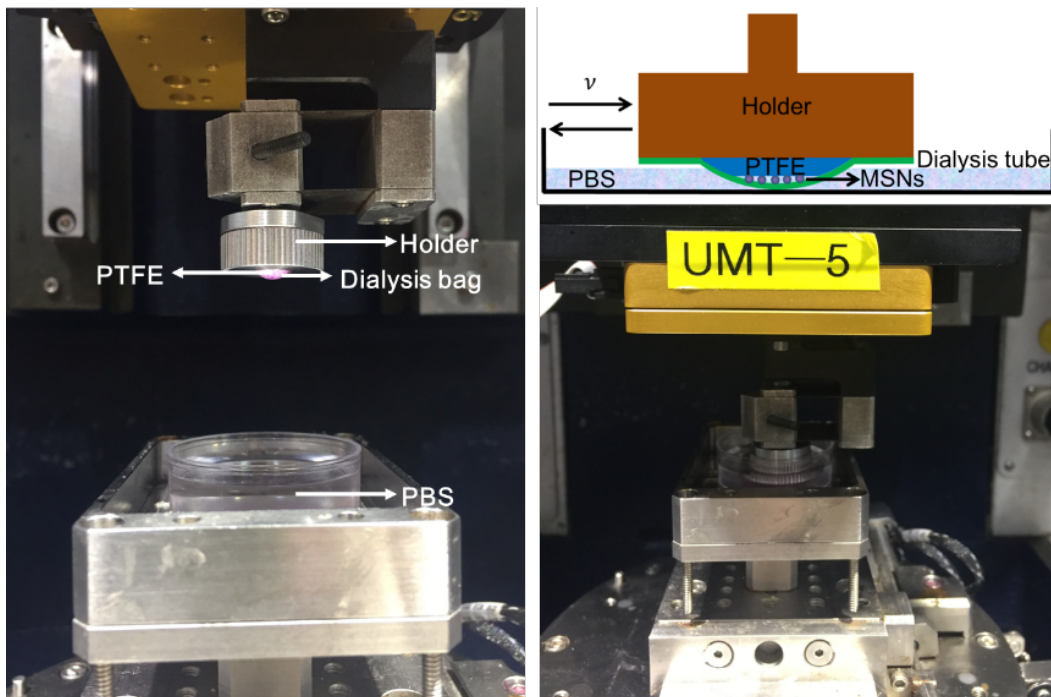

Figure S27. Illustration of friction-activated cargo release tests.

In all the experiments, 2 mL of the medium was taken out from the release buffer for examination and replaced by 2 mL of fresh PBS solution after a predetermined time.

6. Numerical Simulation about Energy Conversion during Dynamic Friction

A numerical method was used to investigate the energy conversion of the simulated joints cavity. The simulation was carried out by ABAQUS using dynamic explicit temperature-displacement coupled model. A snapshot and mesh of model was shown in **Figure S28**. The upper model of the simulated joint surface was a ball with a diameter of 8 mm. The lower model of the simulated joint surface was a flat with the size of 50 mm × 50 mm × 5 mm. Element type for the upper model and the lower model was C3D10MT 10 node mesh and C3D8T 8 node mesh, respectively.
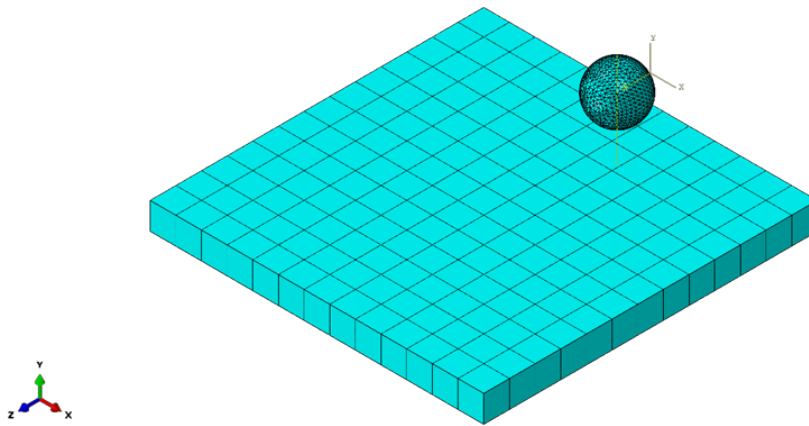

Figure S28. Snapshot and mesh of the model.

The simulated joint surfaces slid against each other without rolling in a reciprocating mode. The contact set was as follows: sliding speed: 16 mm/s; sliding frequency: 2 Hz; oscillation amplitude: 4 mm; normal load: 4 N; COF: 0.3. The parameters used in the simulation were shown in **Table S5**.

Table S5. Parameters of the materials used in the simulation.

Components	Materials	Young modulus (Gpa)	Poisson's ratio	Density (g/cm³)	Specific heat capacity (kJ·kg⁻¹·k⁻¹)	Thermal conductivity (W·m⁻¹·K⁻¹)
The upper model (ball)	PTFE	0.5	0.3	2.2	1.0	0.25
The lower model (flat)	PS	3.2	0.3	1.05	1.3	0.16

The initial temperature was set to 20 °C. The temperature distribution curve of centre longitudinal section after friction of 4.5 s was shown in **Figure S29**. Two extremal points appeared at the edge of the contact area because of the reciprocating movement mode, reaching 50.79 °C. The temperature dropped rapidly as moving away from the contact area.
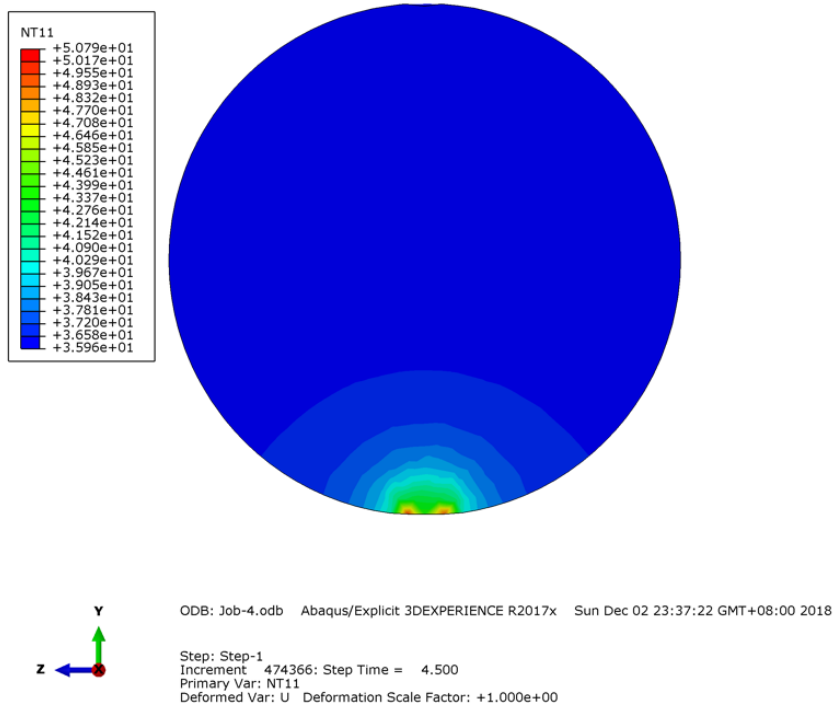

Figure S29. Temperature distribution curve of centre longitudinal section after friction of 4.5 s.

7. *In Vitro* Cytotoxicity

In vitro cytotoxicity of MSNs-NH$_2$, bMSNs and bMSNs⊃SC[4]A was evaluated by CCK-8 assay using mouse embryonic osteoblast precursor (MC3T3-E1) cells. Experiments were executed concerning the procedures of our previously published paper.[S4] A schematic description of the *in vitro* cytotoxicity tests was shown in **Figure S30**. The MC3T3-E1 cells were cultured in a 24-well plate at a density of 3×10^4 cells/well and then incubated in alpha-MEM culture medium supplemented with 10% fetal bovine serum and 1% penicillin-streptomycin for 24 h. After that, the cells were exposed to MSNs-NH$_2$, bMSNs and bMSNs⊃SC[4]A (0.05 mg/mL) and further incubated for 1 day and 3 days. Finally, the CCK-8 working solution was added to the culture medium (100 µL/well), and the cells were incubated for another 3 h.

The results in **Figure S31** showed that the cell viability of the materials was higher than 80% for all incubation times tested, indicating that all the nanoparticles process excellent biocompatibility with the MC3T3-E1 cells. That also displayed these as-made materials were safe for biomedical application.
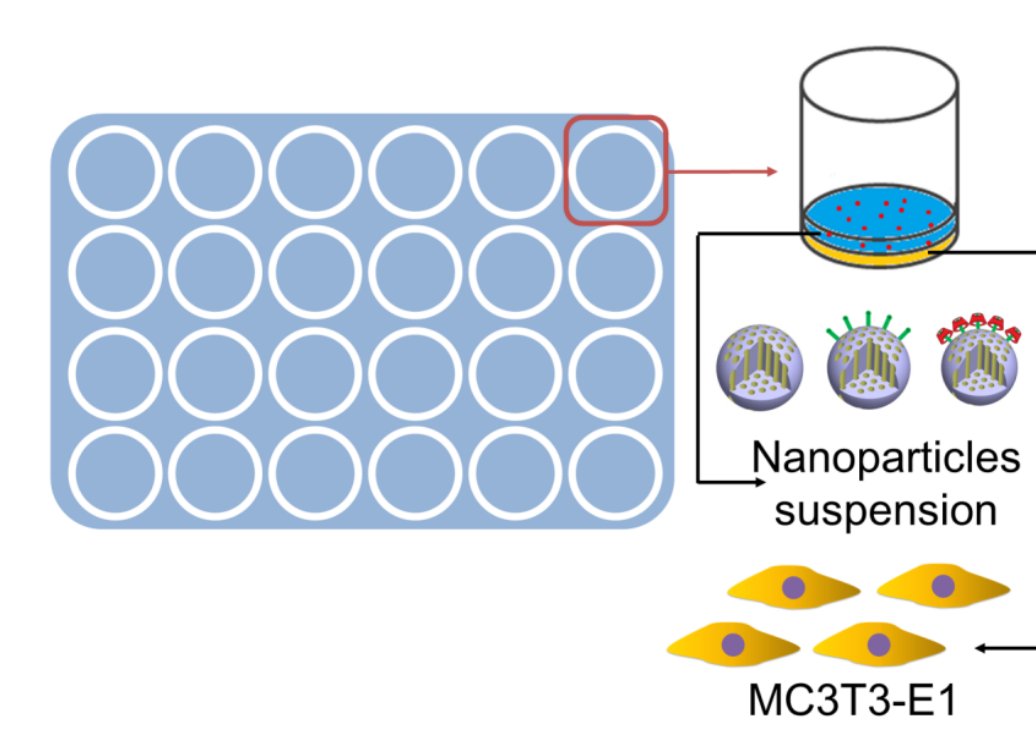

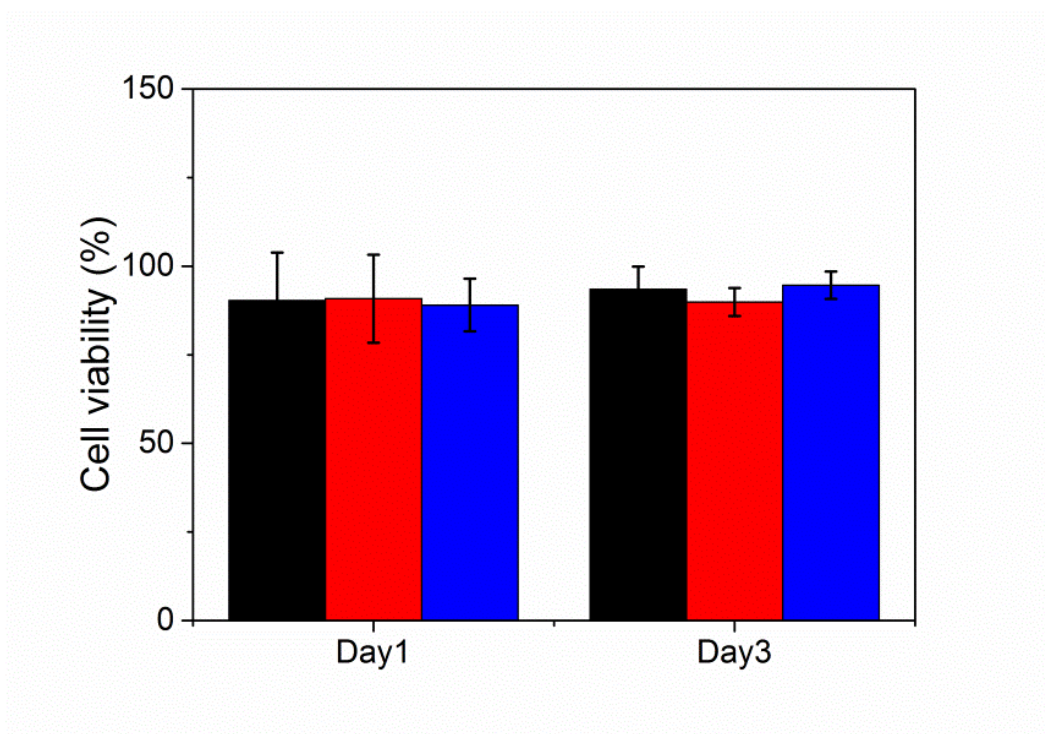**Figure S30.** Illustration of *in vitro* cytotoxicity tests.

Figure S31. The cytotoxicity of MC3T3-E1 mouse calvaria-derived cell line incubated with MSNs-NH$_2$ (black), bMSNs (red) and bMSNs⊃SC[4]A (blue) for 1 day and 3 days.

8. References

1 Y. Sun, Y. Zhou, Q. Li and Y. Yang, *Chem. Commun.*, 2013, **49**, 9033–9035.

2 H. Zhang, Y. Sun, Y. Sun and M. Zhou, *Bio-Med. Mater. Eng.*, 2014, **24**, 2211–2218.

3 S. Jahn, J. Seror and J. Klein, *Biomed. Eng.*, 2016, **18**, 235–258.

4 T. Sun, Y. Sun and H. Zhang, *Polymers*, 2018, **10**, 513–522.